International Journal of Engineering Research & Technology (IJERT)
ISSN: 2278-0181
Vol. 3 Issue 8, August - 2014

Barrelling Aspects and Microstructure Examination of Sintered AISI 8620 P/M Steel during Hot Upset Powder Preform Forging

Y. G. Bala[1]
Ph.D. Scholar

S. RamanSankaranarayanan[2]
Professor & Head

K. S. Pandey[3]
Professor

[1, 2, 3] Department of Metallurgical and Materials Engineering
National Institute of Technology,
Tiruchirappalli -620 015, T.N., India

Abstract - Present investigation is to generate experimental data on AISI 8620 steel through hot axial upset forging in order to reveal the densification mechanisms under bulging and further to examine the microstructural development at different height strains.. Compacts of initial aspect ratios of 0.60, 0.90 and 1.20 were prepared from homogeneously blended powders corresponding to AISI 8620 steel in the pressure range of 480±10M Pa maintaining the density in the range of 85±1% of theoretical. Sintering operation was carried out at 1150 ± 10°C for a period of 90 minutes in an electric muffle furnace under the protection of ceramic coating. Sintered compacts were hot upset forged to various height strains except one sample from each aspect ratio kept as in sintered condition for comparison purposes. Analysis of experimental data, calculated parameters with series of plots and microstructural details have resulted in several empirical relationships relating densification, Poisson's ratio, and new Poisson's ratios while considering typical bulging such as circular and parabolic arcs for the mechanism/s of densification studies.

Keywords: compacts, sintered, barrelling, circular, parabolic, densification, microstructure

1. INTRODUCTION

Powder metallurgy (P/M) is primordial technical method, which produces the parts by compacting the metal powder and then sintering to increase the strength of the part. Since powder metallurgy deals with metal powders, this process had a wider choice for material composition and alloys that might be not possible to produce by other methods [1, 2]. These days, P/M processes draw more attention in two primary areas, namely, one is in density ranges below 7.1 g/cm³ with low to medium strength requirements and the second main application area is fully dense P/M products produced via powder preform forging [3]. Still P/M provides the promising method for commercial production of articles for different purposes such as structural tools, electrical contact materials, and magnetic articles, automotive and automobile components. Apart from these, there are wide spectrum of possibilities of employing the hot powder preform forging methods for the production of components highly suitable for automobile industry, agricultural engineering, railway transport, equipment building and military technology [4]. Powder Preform Forging has developed a proven competence in series production for high strength and high performance products. The companies of USA, Germany, and Japan [5] have created large-scale production of gearbox components, synchronizer rings, and connecting rods through powder forging processes. Many investigators have carried out theoretical analysis and experimental studies on the deformation and densification mechanism/s of powder forging processes [6-12] and justified the enhanced level of densifications attained in powder preform forging operations. A powder based steel plate which are incorporated in manufacturing of brake pads used as backing plate for heavy duty applications was analyzed to execute with very good hot workability, high toughness and heat treated to improve toughness, economy and performance [13]. Powder forging of a connecting rod/s save much material, reduced equipment and remove excessive machining operations. Compared to the conventional fabrication methods, the connecting rod produced by powder preform forging processes not only control the powder weight accurately, but, also can avoid some defects caused in traditional processes and improve the mechanical properties and also provide the good reference for adopting this method of manufacturing for most of the automobiles connecting rods [14]. Market forces in the P/M industry are challenging the traditional compositions typically used in P/M alloys such as Mo, Ni and Cu can be the predominantly used in ferrous P/M parts due to their low affinity for oxygen [15]. Based on the growing progress of powder forging in developing the parts with the required properties by adopting hot deformation processes, an experimental attempt has been made to investigate the densification mechanism/s of a low alloyed silicon, manganese, molybdenum, chromium and nickel high strength AISI 8620 P/M steel. The AISI 8620 alloy steel is a common, low alloy high strength, carburizing alloy steel. This alloy steel is flexible during hardening treatments, thus enabling improvement of case/core properties. The AISI 8620 steels extensively used for a number of medium-strength applications such as camshafts, fasteners, gears, chains and chain pins [16]. The hot upset powder preform forging induces an increased

level of densification from the stage of compaction through to final forging which ranges from 80-85% in compacts to about 99% in the forged products. The deformation and densification also lead to derive some relationships based on deformation considering bulging aspects where the detailed discussion put forth in result and discussion. The criteria for considering the bulging aspect is that the axial upset forging involves the flow of the material in the direction perpendicular to the direction of the deforming forces applied. Hence, the material flow during axial upset forging results in friction between the contact surfaces of the platens and the work-piece which in turn becomes responsible for the bulging of the samples on the free surfaces which could be either circular or with parabolic arcs as described by Narayansamy and Pandey relationships [17, 18]] and Narayansamy and others [19].

In order to analyse the present experimental data and the calculated parameters, the microstructural examinations have also been carried out at the cross sections the of selected forged samples for analyzing the internal morphology with respect to various height strains of the sintered and the forged samples, which supported the strength properties of this AISI 8620 composition as per the standard requirements. Thus, the critical analysis of the present investigation provides a gateway for the approach to investigate this triple alloy nickel, chromium, molybdenum steels through powder preform forging.

2. EXPERIMENTAL DETAILS

2.1 Materials and Tools Required

The materials required to conduct the present investigation are Carbon in the form of graphite powder, silicon, manganese, molybdenum, chromium, nickel and iron powders were procured from the Ghrishma Speciality Powders Limited, Mumbai, and Maharashtra, India. The required per cent age of the elements to yield the AISI 8620 steel composition is tabulated in Table-1. Standard steel pot-mill was used for the blending of these metal powders together in order to obtain the homogeneous powder blend. High- Carbon-High-Chromium mother die, punch along with a suitable bottom insert. The experimental set up for powder compaction is shown in Figure-1 which was used for preparing the initial compacts of required aspect ratios. Graphite powder paste in acetone was used as a lubricant during compaction of the above powder blend on a 1.0 MN capacity UTM. Indigenously developed ceramic coating was also required for the protection of the preforms during sintering in an electrical muffle furnace and a Friction Screw Press was also required for conducting the subsequent hot forging of the sintered preforms.

Table: 1 Composition of Alloys for AISI 8620

Powders	C	Si	Mn	Mo	Cr	Ni	Fe
% Composition	0.2	0.28	0.8	0.2	0.5	0.55	Bal*

Bal.* - Balance

2.2 Preparation of Powder Blend

The preparation of the powder blends for AISI 8620 of required composition mentioned in Table 1 was prepared and blended in the standard steel pot mill along with ceramic balls for a period of 36 hours to obtain homogenous mixture. The ratio of 1:1 for powder to ball weight ratio maintained during homogeneous blending. The 100gm of blended powder taken out from the pot mill for every one hour of the blending and made measurements for its flow rate, tap density, and apparent density using Hall-flow meter for homogeneity of the powder.

2.3 Cold Compaction

The pre – weighed homogeneously blended powders were compacted in a universal testing machine of 1.0MN capacity. The complete compaction assembly is shown in figure -1. The compacts of initial aspect ratios of 0.6, 0.9 and 1.2 of twelve in numbers of each aspect ratios respectively in the high carbon high chromium die of diameter 25mm and the height of 135mm. Prior to compaction, the die, punch and the bottom insert were lubricated with the graphite paste in acetone in order to avoid friction and to obtain good surface finish of the resultant compacts. The required amount of blended powder by weight, was poured into the die with the bottom insert and punch suitably inserted from the top of the die. The powder blend corresponding to AISI 8620 composition was compacted to the required three initial aspect ratios under the applied pressure of 480±10MPa while maintaining the initial fractional preform densities in the range of 0.85±0.01 respectively.

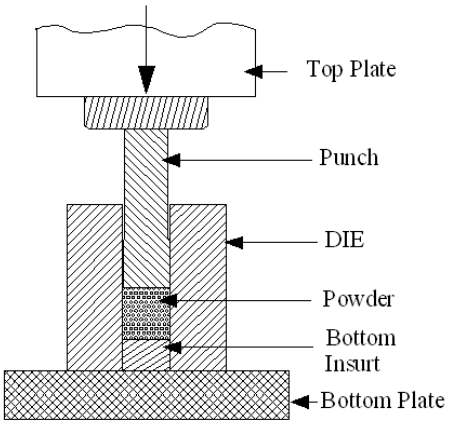

Fig. 1 Compaction Assembly

2.4 Ceramic Coating and Sintering

Indigenously developed ceramic coating was applied over the entire surfaces of the green compacts in order to protect them during sintering at $1150^{o} \pm 10^{o}$C for a period of 90 minutes in an electric muffle furnace against oxidation. This coating was applied in two steps one above the other, but, perpendicular to each other. However, each of the coats were dried for a period of 12hrs independently in an ambient conditions The ceramic coated green compacts after the completion of the drying, schedule were arranged in a high temperature ceramic tray and the tray along with

the coated compacts were placed inside the electric muffle furnace chamber in the uniform temperature zone of 1150°±10°C. Sintering was carried out for a period of 90 minutes at the above temperature.

2.5 Hot Upset Forging

The sintered compacts of three different aspect ratios of 0.6, 0.9 and 1.2 respectively were hot upset forged to different height strains on a 1.0MN capacity Friction Screw Press, except one sample from each aspect ratio was kept as in sintered condition for the reference purposes. These forged preforms were transferred into Linseed oil bath immediately after forging.

2.6 Dimensional Measurements

The oil-quenched forged samples were cleaned properly while removing any residual coating from the compact forged preforms. The dimensional measurements such as the forged heights (H_f), contact diameters (top (D_{c1}) & bottom (D_{c2})) and bulging diameter (D_b). Minimum four readings of the above mentioned parameters were taken and then averaged out. Density of the sintered and forged samples were also measured using Archimedean's principle, considering the density of water as 1gm /cc. Using these measured parameters, diameter strains, height strains, bulging, Poisson's ratio considering no barrelling and circular and parabolic barrelling modes were calculated.

3. RESULTS AND DISCUSSIONS

Based upon the theoretical analysis by Narayansamy and Pandey relationships [17-19] for porous preforms, experimental data and calculated parameters have been utilized to establish various relationships relating to fractional theoretical density with respect to height strain, diameter strain, bulging ratio and new Poisson's ratios considering circular and parabolic arc of bulging which are discussed in the subsequent sections.

3.1. Deformation, Densification and Height Strains

Figure - 2 is the plots drawn between fractional theoretical density (ρ_f/ρ_{th}) and the true height strain exhibiting the influence of initial preform geometry during hot upset forging of the sintered preforms of AISI 8620 for three different aspect ratios, namely, 0.6, 0.9 and 1.2 respectively. The observation these curves clearly demonstrates that they possess similar characteristic features and, therefore, they are expected to conform a similar mathematical

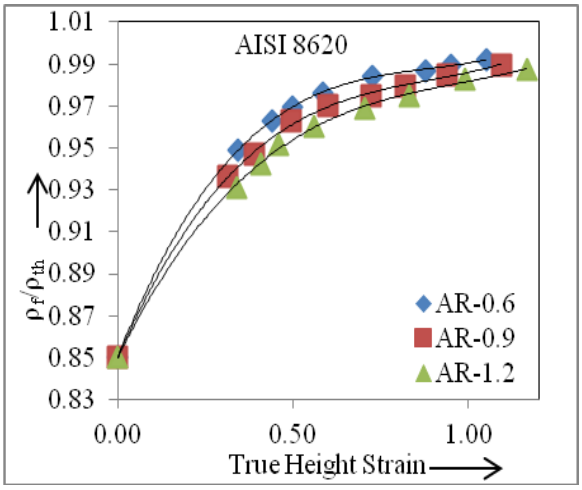

Fig 2 Effect of Initial Aspect Ratio (H_0/D_0) on the Relationship between Fractional Theoretical Density and the True Height Strain.

expression and the same was found to conform to a third order polynomial of the form: $(\rho_f/\rho_{th}) = a_3\varepsilon_h^3 + a_2\varepsilon_h^2 + a_1\varepsilon_h + a_0$, where, (ρ_f/ρ_{th}) is the fractional theoretical density, ε_h being the true height strain, i.e., $\varepsilon_h = \ln (H_o/H_f)$, '$a_0$', '$a_1$', '$a_2$' and '$a_3$' are found to be empirically determined constants and are further found to depend upon the initial preform geometries. These constants are tabulated in Table -2. The values of 'a_0' for all aspect ratios are found to be in very much close proximity to initial preform densities which lied in between 0.85±0.01, and, therefore, did not contribute to densification in any form.

Table 2 Coefficient of constants of the form: $(\rho f/\rho th) = a_3\varepsilon h^3 - a_2\varepsilon h^2 + a_1\varepsilon_h + a_0$

AR	a_0	a_1	a_2	a_3	R^2
0.6	0.85	0.42	-0.45	0.17	0.99
0.9	0.85	0.38	-0.39	0.15	0.99
1.2	0.85	0.34	-0.31	0.11	0.99

However, the values of 'a_1' and 'a_3'were found to be positive and in descending order as the aspect ratios were increased, and, therefore, these constants assisted densification. The constant 'a_1' linearly enhanced the densification as it are multiplied by the true height strain. In this period, only a maximum densification attained for the preforms. Further the 'a_2'values were found to be negative and are multiplied by the square of true height strain which has been always less than unity value. Therefore, this constant will assist densification only moderately. Thus this constant only smoothen the curves in the final stages of densification. The values of these constants are shown in the Table -2. Further, the preform of lower aspect ratios densified more conclusively compared to larger aspect ratio preforms because the forging load transferred across the height direction is more rapid with less damping compared to larger aspect ratio preforms experience higher damping into poor densification. The 'R^2' value for each aspect ratio and for each composition is extremely close to unity and hence the equation proposed is justified.

3.2. Deformation, Densification and Diameter Strains

Figure 3 is the plot drawn between the fractional theoretical density and the true diameter strain during the hot forging deformation of sintered AISI 8620 steel showing the influence of initial aspect ratio. Carefully observing the curves, it follows the similar characteristic nature of the previously discussed true height strain curves. The preform of lower aspect ratios densified more conclusively compared to larger aspect ratio preforms because the lower aspect ratio experienced the forging load transferred across the diameter strain direction is more rapid with less damping compared to larger aspect ratio preforms experience higher damping into poor densification. The nature of the characteristics curves follows a nature of the polynomial form of fourth order, is given by $(\rho_f/\rho_{th}) = -b_4\varepsilon_d^4 + b_3\varepsilon_d^3 - b_2\varepsilon_d^2 + b_1\varepsilon_d + b_0$, Where, ε_d is the true diameter strain

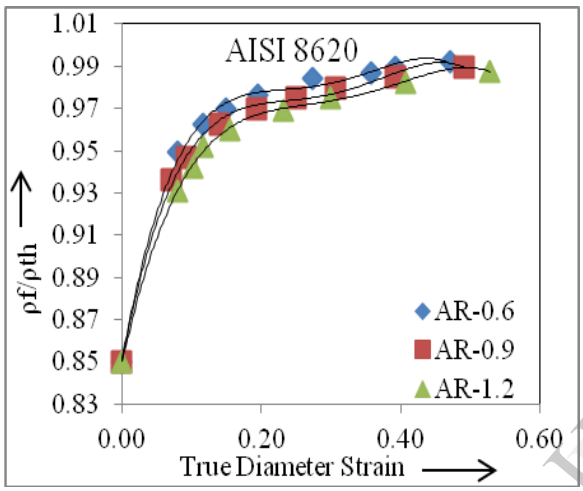

Fig. 3 Effect of initial aspect ratio (H_0/D_0) on the relationship between fractional theoretical density and true diameter strain

density and 'b_0', 'b_1', 'b_2', 'b_3' and 'b_4' are found to be empirically determined constants are tabulated in Table-3. From this 'b_2' 'and 'b_4' are found to be negative which assist moderately for densification as the true diameter 'strain ($\ln (D_c/D_0)$) is raised, (ρ_f/ρ_{th}) is the fractional theoretical b_1' and 'b_3'are found to be positive value and are in the decreasing order with respect to the lower aspect ratio to higher aspect ratio, which influences in such a manner that the lower aspect ratio preforms are comparatively more densified the larger aspect ratio preforms. The value of 'b_0' is close to the initial preform density 85±1 per cent, and, therefore, it does not contribute in any form to densification. The polynomial order proposed above stands justified since the regression coefficient R^2 value is in very much close proximity to unity and therefore these curves are the best fit curves. The constant b_1 and b_3 are positive and, therefore they contribute to densification, whereas, the constants b_2 and b_4 are negative, and, therefore, they tend to flatten the curves in the final stages of their journey.

Table: 3 Coefficient of the constant of the form: $(\rho_f/\rho_{th}) = -b_4\varepsilon_d^4 + b_3\varepsilon_d^3 - b_2\varepsilon_d^2 + b_1\varepsilon_d + b_0$

AR	b_0	b_1	$-b_2$	b_3	$-b_4$	R^2
0.6	0.85	1.83	9.86	23.13	19.36	0.997
0.9	0.85	1.70	8.91	20.39	16.60	0.998
1.2	0.85	1.48	6.97	14.57	10.91	0.994

3.3 Relation between New Diameter Strain and the True Height Strain (Circular Arc as well as for Parabolic Arc)

Figures -4(a) and 4(b) are the plots drawn between the fractional theoretical density (ρ_f/ρ_{th}) and the new diameter strains considering circular and parabolic arc of barrelling for the forged preforms

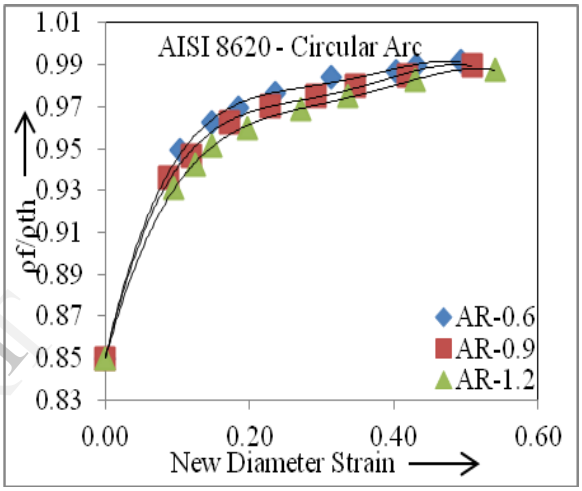

Fig-4(a) Effect of Initial Aspect Ratio (H_0/D_0) on the Relationship between Fractional Theoretical Density and New Diameter Strain for Circular Arc of Barrelling.

of AISI 8620 composition. Similar Characteristic natures of the curves are obtained as were obtained between the fractional theoretical density and the true diameter strains for general mode of barrelling as the same is discussed above. Hence, the similar mathematical expression can be proposed for the circular and parabolic arcs of barrelling's as well. Thus, a similar fourth order mathematical equation is empirically arrived in these two cases as well and the same is expressed as given beneath:

$$(\rho_f/\rho_{th}) = c_4\varepsilon_{dnew}^4 - c_3\varepsilon_{dnew}^3 + c_2\varepsilon_{dnew}^2 - c_1\varepsilon_{dnew} + c_0$$

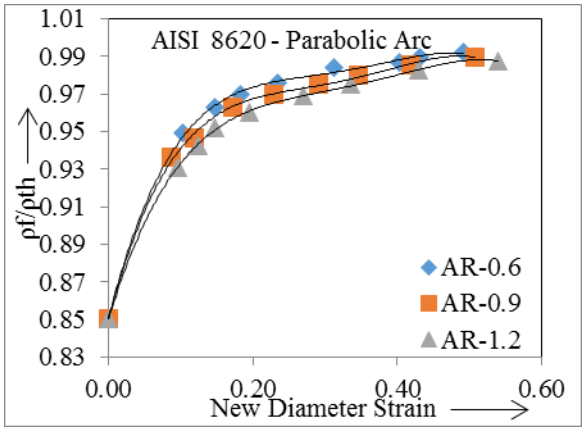

Fig-4(b) Effect of Initial Aspect Ratio (H_0/D_0) on the Relationship between Fractional Theoretical Density and New Diameter Strain for Parabolic Arc of Barrelling.

Where 'c_0', 'c_1', 'c_2', 'c_3'and 'c_4' are the empirically determined constants and the ε_{dnew} is the new diameter strain considering circular and parabolic arcs respectively. The equation is justified since their regression coefficient values of R^2 has almost reached to unity, and, therefore, the above curves are the best fit curves. The coefficients of the fourth order polynomial along with the regression coefficients are tabulated in Table – 4. Since, the values of 'c_0' in each case is found to be the initial preform density, hence, did

Table: 4 Coefficient of the constant of the form: $(\rho_f/\rho_{th}) = c_4\varepsilon_{dnew}^4 - c_3\varepsilon_{dnew}^3 + c_2\,\varepsilon_{dnew}^2 - c_1\,\varepsilon_{dnew} + c_0$

B	AR	$-c_1$	c_2	$-c_3$	c_4	c_5	R^2
CA	0.6	10.55	14.05	6.84	1.51	0.85	0.998
	0.9	10.51	13.88	6.64	1.44	0.85	0.999
	1.2	7.39	10.36	5.31	1.26	0.85	0.999
PA	0.6	10.57	14.08	6.85	1.51	0.85	0.998
	0.9	10.52	13.89	6.64	1.44	0.85	0.999
	1.2	7.39	10.36	5.32	1.27	0.85	0.999

B = Barrelling; CA = Circular Barrelling and PA = Parabolic Barrelling

not contribute to densification as well as to barrelling. Further the constants 'c_2'and 'c_4' are both negative, and, hence, they tend to flatten the curves in their final stages of densification and deformation. However, the positive values of 'c_1'and 'c_3' did contribute to densification on deformation and bulging

3.4 Deformation Leading to Changes in True Diameter and Height Strains

Figures 5(a), 5(b) and 5(c) are the plots drawn between the true diameter strains and the true height strains during hot deformation of sintered AISI 8620 steel showing the influence of initial aspect ratio considering the general ,circular and parabolic arc of barrelling . Observing the curves plotted in each of these figures, it is found that they followed a similar characteristics nature and all data points positioned themselves below the theoretical line of slope as one half irrespective of the initial preform geometries. This clearly indicates the fact that the value of Poisson's ratio will never reach to its theoretical value of 0.5 and therefore this makes to conclude that the sintered preforms would never densify to cent per cent density under the upsetting mode of deformation. In each of these figures, the curves corresponding to least aspect ratio preforms always remains above, the larger aspect ratio preforms. In fact, the curves corresponding to the larger aspect ratio preforms always remained below the curves corresponding to the lower aspect ratio preforms, i.e., it remained farthest away from the theoretical line at the farthest away from the theoretical line, and the curves corresponding to medium sized aspect ratio preforms remained in the middle of above two curves. All these curves have been found to conform to a third order polynomial of the form: $\varepsilon_d = -f_3\varepsilon_h^3 + f_2\varepsilon_h^2 + f_1\,\varepsilon_h - f_0$., Where, '$f_3$', '$f_2$', f_1'and 'f_0' are found to be empirically determined constants and they do depend upon the composition and initial geometries of the preforms. ε_d is the true diameter strain and ε_h is the true height strain .

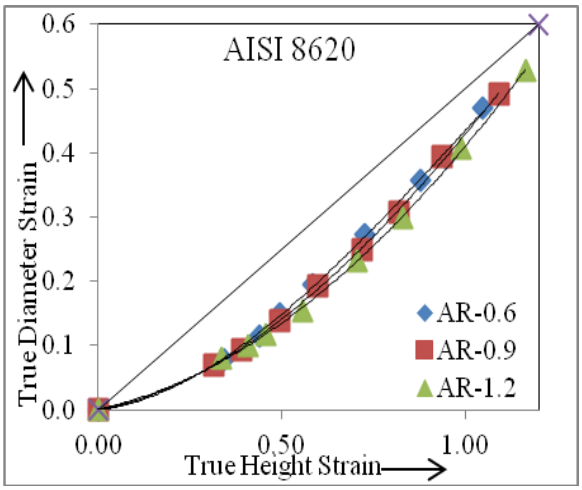

Fig. 5(a) Effect of Initial Aspect Ratio (H_0/D_0) on the Relationship between Fractional True Diameter Strain and True Height Strain.

Examining these curves and the corresponding equations, the constants are tabulated in Table -5. Observing this table carefully, it is found that the constant 'f_0' is nearly zero justifying the stand that at no deformation, there is no height strain or diameter strains.'f_1'and 'f_0' are found to be empirically determined constant and they do depend upon composition and initial geometry of the preforms. ε_d is the true diameter strain and ε_h is the true height strain .

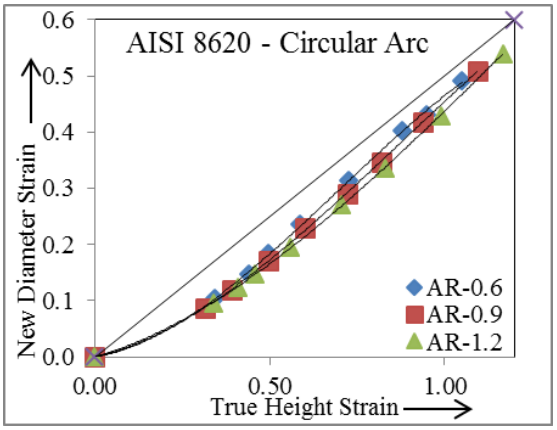

Figure 5(b) Effect of Initial Aspect Ratio (H_0/D_0) on the Relationship between Fractional New Diameter Strain and True Height Strain for Circular Arc.

Further'f_2', and 'f_1' are positive and their contribution to the rise in the values of diameter strain as height strain is raised. However in the case of constant 'f_3' mostly its value are negative hence it acts to moderate the values of diameter strain Since, the regression coefficient 'R^{2}' values are found in the close proximity of unity, and, hence, the above equation is valid for relating ε_d and ε_h for all aspect ratios while taking 'f_0'= 0, the equation is modified as under: $\varepsilon_d = f_3\varepsilon_h^3+f_2\varepsilon_h^2+f_1\varepsilon_h$. Similar way the same the diameter strain and height strain achieved for the deformation considering the circular arc and parabolic arc of barrelling which are shown in the figures (5b) and figure (5c). The characteristic curve of the respective aspect ratio followed the similar form of the third order polynomial, which is justified by its regression coefficient R^2 values which are in close proximity to unity. Thus, the curves are the best fits. These constants are tabulated in Table -5.

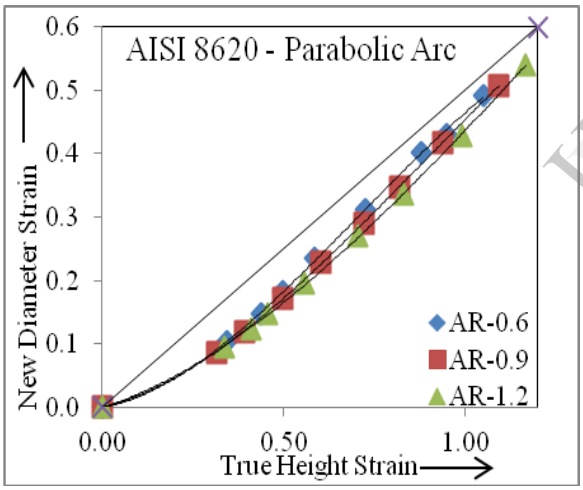

Fig. 5(c) Effect of initial Aspect ratio (H_0/D_0) on the relationship between New Diameter Strain and True Height Strain for Parabolic Arc.

Table: 5 Coefficient of the constant of the form: $\varepsilon_d=-f_3\varepsilon_h^3+f_2\varepsilon_h^2+f_1\varepsilon_h- f_0$

Barl*	AR	$-f_3$	f_2	f_1	$-f_0$	R^2
Gen*	0.6	0.18	0.54	0.07	-0.0007	0.99
	0.9	0.07	0.40	0.09	0.0002	0.99
	1.2	0.01	0.29	0.12	0.0008	0.99
CA*	0.6	0.33	0.68	0.10	-0.0004	0.99
	0.9	0.18	0.50	0.14	-0.0004	0.99
	1.2	0.09	0.35	0.18	-0.0005	0.99
PA*	0.6	0.33	0.69	0.11	-0.0004	0.99
	0.9	0.18	0.50	0.14	-0.0004	0.99
	1.2	0.09	0.35	0.18	-0.0005	0.99

Barl* - Barrelling; Gen*- General;
CA*- Circular Arc; PA*- Parabolic Arc

3.5. Poisson's Ratio and Densification

Figures- 6(a), 6(b) and 6(c) represent the plots drawn between Poisson's Ratios (γ_p) with the fractional theoretical density showing the influence of initial preform geometries considering general, circular and parabolic arcs of barrelling. While examining the curves in each of these figures, it is found that the curve corresponding to the largest aspect ratio preforms are much above the curves corresponding to the lower aspect ratio performs. Since all these curves are found to be characteristically similar in nature, therefore, they must conform to a similar form of a mathematical equation. However, the curve fitting technique has yielded a third order polynomial when represented between the Poisson's ratio (γ_p) and the fractional theoretical density of the form: $\gamma_p = g_3(\rho_f/\rho_{th})^3+ g_2(\rho_f/\rho_{th})^2+ g_1(\rho_f/\rho_{th}) +g_0$. Since '$g_1$' and '$g_3$' are negative, and, therefore, they do not contribute to densification even though the values of the Poisson's ratio, i.e., γ_p is on the increasing trend. These curves can be split into two segments of density, where, there is a rapid rise in density, but, a slow increase in the values of the Poisson's ratio, γ_p. But, in the second segment, there is a rapid rise in the values of the Poisson's ratio, but, a low increase in densification. Therefore, it can be comprehensively established that in this region the flow of pores and the materials, both become simultaneous. However, the constants 'g_2' and 'g_4' are positive and, therefore, they contribute to an increased rates of densification as well as rise in the values of the Poisson's ratio. All these constants are tabulated in Table -6. In view of the above argument, the mathematical relationship earlier proposed stands justified. Since, the values of the regression coefficient in each case is above 0.999 which is almost equal to unity. Hence, the above justification.

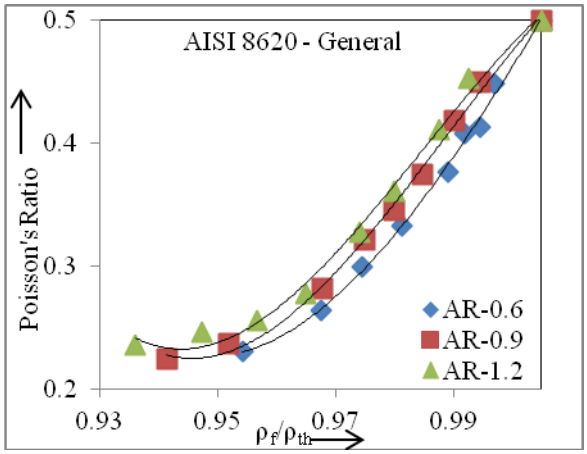

Fig 6(a) Effect of Initial Aspect Ratio (H_0/D_o) on the Relationship between Poisson's Ratio and Fractional Theoretical Density.

Similarly, figures for circular and parabolic arcs of barrelling drawn between new Poisson's ratio (γ_p') and the relative density (ρ_f/ρ_{th}) can be explained on the similar lines as is expressed in case of the general mode of bulging. Here, too, the curves followed a third order polynomial with the empirically determined constants 'g_0', 'g_1', 'g_2' and 'g_3' are listed in Table -6. Here, too, the values of Regression coefficients for each curve are found to be in very much close proximity to unity. Hence, the third order polynomial expressed above do stand valid for the relationship between the new Poisson's ratio considering the circular (γ_p') and the parabolic (γ_p'') arcs of barrelling and (ρ_f/ρ_{th}) in the similar way of the above equation.

Table: 6 Coefficient of the constant of the form: $\gamma_p = g_3 (\rho_f/\rho_{th})^3 + g_2 (\rho_f/\rho_{th})^2 + g_1(\rho_f/\rho_{th}) + g_0$

Barl*	AR	$-g_3$	g_2	$-g_1$	g_0	R^2
Gen*	0.6	542.9	1654	1671	560.5	0.99
	0.9	1115	3293	3235	1057	0.99
	1.2	1177	3460	3385	1102	0.99
CA*	0.6	1229	3606	3522	1145	0.99
	0.9	674.6	1975	1923	623.1	0.99
	1.2	463.9	1361	1328	431.1	0.99
PA*	0.6	1225	3594	3510	1141	0.99
	0.9	667.3	1984	1932	626.1	0.99
	1.2	469.0	1377	13435	436.0	0.99

Barl* - Barrelling; Gen*- General;
CA*- Circular Arc; PA*- Parabolic Arc

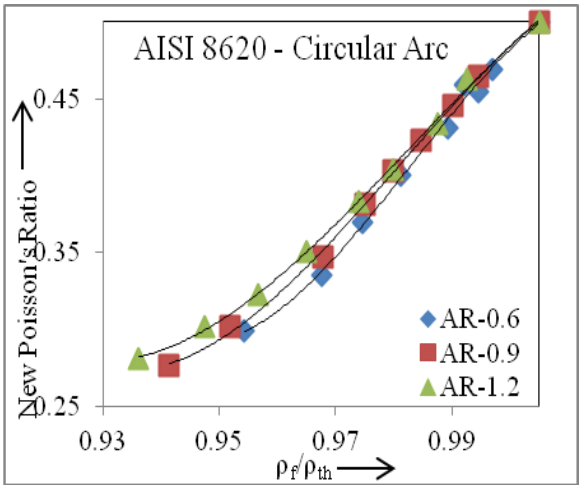

Fig 6(b) Effect of Initial Aspect Ratio (H_0/D_o) on the Relationship between Poisson's Ratio and Fractional Theoretical Density for Circular Arc.

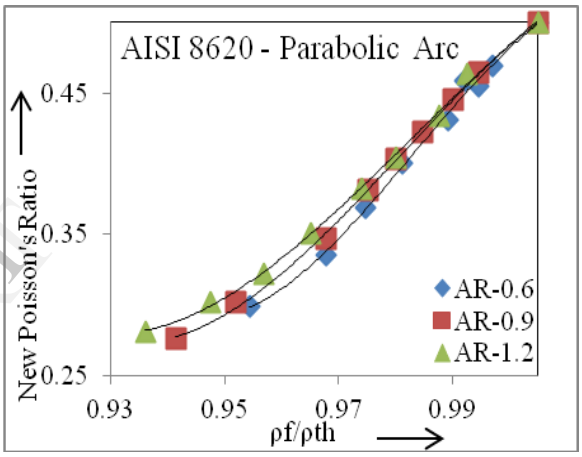

Fig. 6(c) Effect of Initial Aspect Ratio (H_0/D_o) on the Relationship between Poisson's Ratio and Fractional Theoretical Density for Parabolic Arc

3.6 Deformation, Densification and Bulging

Figures 7 (a) and 7 (b) show the plots drawn between fractional theoretical densities (ρ_f/ρ_{th}) and the bulging ratio (D_b/D_0) and log (% Fractional theoretical density) versus log (bulging ratio). The characteristic nature of the curves in figure -7(a) is found to be quite similar to each other, and, therefore, they must be mathematically expressed by a general relationship of the same form. In fact for all these three different aspect ratios, it was found that a fourth order polynomial of the form: $(\rho_f/\rho_{th}) = h_4 (D_b/D_0)^4 + h_3 (D_b/D_0)^3 + h_2 (D_b/D_0)^2 + h_1 (D_b/D_0) + h_0$ was the most appropriate. Where, 'h_0', 'h_1','h_2', 'h_3', and 'h_4'are empirically determined constants and they are found to depend upon the initial preform geometries. These constants are tabulated in Table -7. The values of 'h_0', 'h_2'and 'h_4' are negative, which imply that their influence had negative contribution to bulging. However, the values of 'h_1' and 'h_3' are positive, and, therefore, they contribute to bulging, and their values are in decreasing order with respect to smaller aspect ratio to higher aspect ratio preforms. This characteristic nature shows that the smaller aspect ratio preforms densified more compared to the larger

aspect ratio preforms. Since the regression coefficient ('R^2') values are either unity or in very much close proximity to unity, and, therefore, these plots exhibit almost ideal fits.

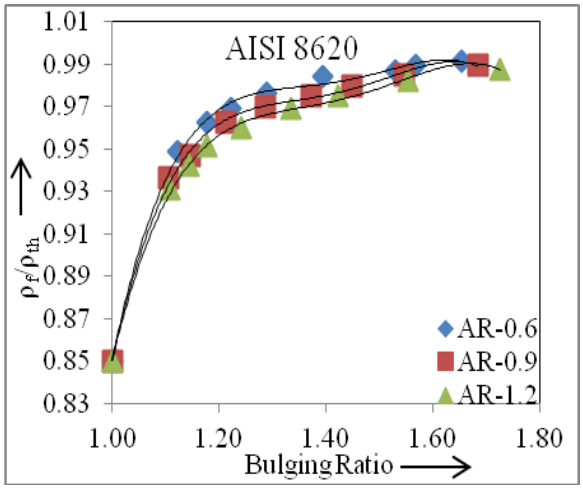

Fig. 7(a) Effect of Initial Aspect Ratio (H_0/D_o) on the Relationship between Poisson's Ratio and Fractional Theoretical Density for Parabolic Arc.

Figure- 7(b) is the plot drawn between the log (% fractional theoretical density) and the log (Bulging Ratio) exhibiting the effect of initial aspect ratio (H_0/D_0) for AISI 8620 sintered P/M steel during hot upset forging. These plots show the characteristics nature of straight line equation as: Log (%FTD) = m {Log (D_b/D_o) + Log (q) in two distinct segments, where, q = Anti {Log (c_1 or c_2)} or Log (q) = c_1 or c_2, and, m = m_1 or m_2 which are the slopes of the lines in segment 1 and 2 respectively. The straight line equations are shown in two segments, one starting from the sintered density, i.e., 85 per cent to the forged density of 95% and the second segment of straight line is from about 95% to the final preform forged density of nearly 99% plus. The constants, i.e., the slopes and the intercepts of the straight lines in both the segments are represented by 'm_1', 'c_1'and 'm_2', 'c_2' respectively, and these constants are tabulated in

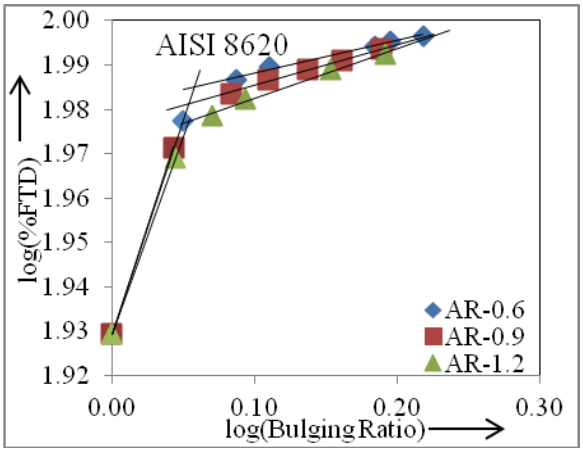

Fig. 7(b) Effect of Initial Aspect Ratio (H_0/D_o) on the Relationship between Poisson's Ratio and Fractional Theoretical Density for Parabolic Arc.

Table-7. Examining the values of the constant 'c_1' for all preforms of three different aspect ratios, it is observed that the same is equal to the initial preform sintered density and for the constant 'c_2' for all the preforms are in the decreasing order, which confirms the densification is higher for the smaller aspect ratios compared to the densification taking place in the larger aspect ratio preforms. This straight-line equation is justified since the regression coefficients for the first segment is almost unity and for the second segment is much closer to unity. Further converting the double logarithmic straight line equation into another mathematical form, it turns out to be a power law equation of the form as is given beneath:

$$\% \text{ (FTD)} = (q_1 \text{ or } q_2) \text{ X } (D_b/D_o)^{(m_1 \text{ or } m_2)}$$

Where, $\mathbf{m_1}$ **and** $\mathbf{m_2}$ are the slopes of the straight lines in the respective segments 1 and 2 respectively. The constants (q_1 or q_2) are equal to anti (Log of c_1 or anti (Log of c_2) depending upon the segment being considered. Thus, % (FTD) can also be expressed by a power law of the bulging ratio ((D_b/D_o) as is given above.

Table: 7 Coefficient of the constant of the form: Y = m x + c

AR	m_1	c_1	R^2	m_2	c_2	R^2
0.6	0.96	1.93	1	0.073	1.98	0.99
0.9	0.97	1.93	1	0.092	1.98	0.99
1.2	0.89	1.93	1	0.113	1.97	0.99

4. Evaluations of Microstructure for Selected Forged Preforms

Microstructure evaluation was examined for some of the selected disc shaped forged samples of smaller aspect ratios at its cross section, which are forged to the level of different height strains and one preform is being taken as in the sintered condition and all were examined at 400X which are shown in figure (8). Figure 8(a) represents the microstructure of the sintered preform and figures 8(b) and 8(c) represent the microstructures of the preforms forged at two different height strains. However, figure 8(d) represents the microstructure of almost fully densified, i.e., at 99.9% attained fractional theoretical density. The microstructures of all preforms reveal the basic major constituents consisting of grains of ferrite and pearlite with differently refined structures when examined at differently height strained conditions. Figure 8(a) shows the microstructure of the sintered AISI 8620 P/M steel preform which exhibits well developed large, but, coarse grains of irregular shapes with substantially high amount of porosities well in compliance of its theoretical density. Figure 8(b)

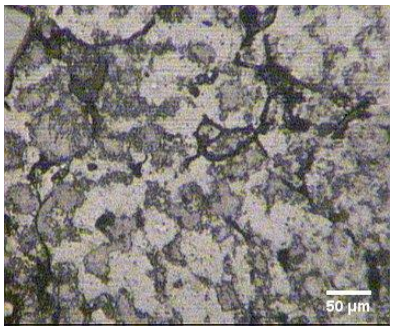

Fig 8(a) Sintered Preform at 400 Magnification

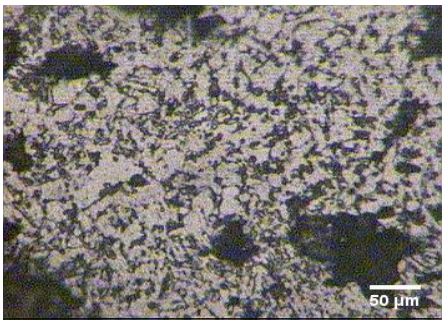

Fig 8(b) Forged Preform at Initial Height Strain at 400 X.

Fig 8(c) Forged Preform at Intermittent Height Strain at 400 X.

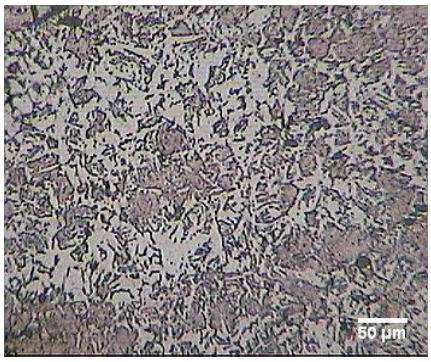

Fig 8(d) Forged Preform of Fully Densified at 400 X.

shows the microstructure of the initially forged disc to a level of 35.3% of height reduction in which grains are refined substantially compared to sintered sample. Figure 8(c) shows the microstructure of the disc forged to height reduction of 44.5%. This structure mainly consists of austenite and scattered ferrite along with fairly reduced level of porosities compared to one exhibited by the previous forged sample. The grains tended to be more refined and well developed. However, figure 8 (d) shows the microstructure of the almost fully densified. The microstructure is fully developed revealing the flattening of grains in the direction perpendicular to the applied loads of deformation. Apart from these, the traces of pores present in the structure also got heavily flattened. Thus, the overall microstructure reveals the fibrous one in its characteristic features. In order to attain improved mechanical properties, suitable heat treatments such as homogenising in the austenitic zone and then quenching them in a desired media followed by a suitable tempering operation.

5. CONCLUSIONS

Critical examination of the experimental data and the calculated parameters and series of graphs plotted along with the analysis of the microstructures developed for AISI 8620 sintered and hot forged preforms through powder preform forging considering deformation and densification under hot upset forging have yielded the following salient conclusions:

1. Densification during hot upset forging of sintered AISI 8620 P/M steel preforms have established that the preforms corresponding to lower aspect ratios have densified at a much faster rates compared to the preforms of larger aspect ratios. This is attributed to the fact that during deformation, the load transfer across the axial direction is more uniform and quick in lower aspect ratio preforms due to the reduced level of damping effect compared to the larger aspect ratio preforms which offered increased resistance to deformation due to increased pore bed height even though the initial preform density for all compacts are the same. Further the characteristics of all densification curves are quite similar to each other, and, therefore, curve fitting techniques employed has yielded a third order polynomial of the form: $\mathbf{(\rho f/\rho th) = a_3\varepsilon h^3 - a_2\varepsilon h^2 + a_1\varepsilon_h + a_0}$, where. ($\rho_f/\rho_{th}$) is the fractional theoretical density, $\varepsilon_h = \ln (H_o/H_f)$, '$a_0$', '$a_1$', '$a_2$' and '$a_3$' are found to be empirically determined constants and are further found to depend upon the initial preform geometries.
2. The characteristics nature of the curves plotted between the fractional theoretical density with respect to the true diameter strains considering the no bulging and bulging at the periphery of the preforms resembling as circular and, or, parabolic arcs during deformation are similar, and, they were also found to conform to a fourth order polynomial with the regression coefficient almost approaching to unity justifying that the curves were the best fit ones. The mathematical relationships arrived in each of the cases is expressed by a single expression of the form as given below :
$\mathbf{(\rho_f/\rho_{th}) = -b_4\varepsilon_d^4 + b_3\varepsilon_d^3 - b_2\,\varepsilon_d^2 + b_1\,\varepsilon_d + b_0}$, where all symbols carry their usual meanings as is described in the text.
3. The relationship between the true diameter strains and the true height strains and also between the Poisson's ratio and the fractional theoretical density considering conventional, circular and parabolic arc of bulging during deformation, also conformed to a third order polynomial with the regression coefficient almost equaling to unity confirming to the best possible curve fits. The relationship established are provided beneath:
$\mathbf{\varepsilon_d = -f_3\varepsilon_h^3 + f_2\varepsilon_h^2 + f_1\,\varepsilon_h - f_0}$ **; and,**
$\mathbf{\gamma_p = g_3\,(\rho_f/\rho_{th})^3 + g_2\,(\rho_f/\rho_{th})^2 + g_1(\rho_f/\rho_{th}) + g_0}$, where, symbols have their usual meanings as are explained in the text and all explanations with reference to them stand valid.
4. The relationship between the fractional theoretical density and the bulging ratios conformed to a fourth order polynomial of the form as is given underneath:

$(\rho_f/\rho_{th}) = h_4 (D_b/D_0)^4 + h_3 (D_b/D_0)^3 + h_2 (D_b/D_0)^2 + h_1 (D_b/D_0) + h_0$; Where, 'h_0', 'h_1','h_2', 'h_3', and 'h_4'are empirically determined constants and they are found to depend upon the initial preform geometries. The regression coefficient of the in each case have been found to approach to unity justifying the fact that this fourth order polynomial relationship arrived at is the most appropriate relation which could be established by the curve fitting techniques.

5. The relationship between the logarithmic (%Fractional theoretical density) and the logarithmic (Bulging Ratio) fits to the straight line relating the linear relationship between them, with the regression coefficient almost equal to the unity. However, Further converting the double logarithmic straight line equation into another mathematical format, it turned out to be a power law equation of the form as is given below:

$\%\ (FTD) = (q_1 \text{ or } q_2)\ X\ (D_b/D_o)^{(m_1 \text{ or } m_2)}$ Where, m_1 and m_2 are the slopes of the straight lines in the respective segments 1 and 2 respectively. The constants (q_1 or q_2) are equal to anti (Log of c_1 or anti (Log of c_2) depending upon the segment being considered. Thus, % (FTD) can also be expressed by a power law relationship with the bulging ratio ((D_b/D_o), and, the same is given as above.

6. The microstructure for the selected preforms have clearly established the growth of the grains and subsequent elimination of the pores present in the preforms on an increased deformations. Developments of grains of ferrite as well as of the austenite have been gradual, but, definite as the densification advanced. However, in the final stages of densification, a banded (fibred) microstructures were observed showing quite high degree of upsetting nearly 65-70% of height reduction with almost nil porosity, an indication of improved properties. In order to obtain improved mechanical properties, suitable heat treatments such as homogenising in the austenitic zone and then quenching them in a desired media followed by a suitable tempering operation. Thus, various automobile components at different density levels with well controlled microstructures and properties can be produced via this route from sintered AISI 8620 steel preforms.

Thus, the present investigation on AISI 8620 P/M steel preforms can be successfully utilized to develop large number of automobile components via hot upsetting forging or semi-closed or in a closed die forgings would be a of a greater utility and successfully meeting the forth-com challenges experienced by the automobile industries with always hunting for newer and newer materials while utilizing the latest technology of the powder preform forging to achieve the best results. It is, therefore, the responsibility of the researchers and the metallurgists to promote and encourage this endeavor for industries to adopt this process of production with series of trial runs.

6. REFERENCES

[1]. J. Georgiev, T. Pieczonka, M. Stoytchev and D. Teo- dosieve, "Wear Resistance Improvement of Sintered Structure Parts By C7h7 Surface Carburizing", Surface and Coatings Technology, Volume. 180-181, 2004, pp. 90-96.

[2]. H. Dong, J. Hu, H. Wang, S. Liu and Z. Guo, "A Study on Carbon Concentration Distribution and Microstructure of P/M Materials Prepared By Carburizing", Journal of Materials Processing Technology, Vol. 49, No. 4, 2009, pp. 3776-3782.

[3]. Richard Slattery, Francis G. Hanejko, Arthur J. Rawlings, Mike Marucci and Kalathur Sim Narasimhan , " High Performance Gears Using Powder Metallurgy (P/M) Technology", Gear Technology Article -Nov/Dec 2004 pp 39-46.

[4]. T.M.Pavlygo, A.V.Sakhnenko, S.A. Sahnenko and GG.Serdyuk "Powder-Metallurgy Industry, Economics, and Organization of Production Development of Powder Material Hot Forging in the Ukraine", UDC 621.762. Powder Metallurgy and Metal Ceramics, Volume. 39, No. 3-4, 2000.

[5]. W. J. Huppman, "The Technical and Economic Development of Powder Forging", Powder Metallurgy International, Volume 24, No. 3, pp 286-293-1992.

[6]. ZHAO Zhongzhi, HUA Lin, WANG Huachang, "The Forming and Densification of Sintered Powder Materials", International Journal Science of Sintering, 1987, Volume 19, No. 2 pp 65-80.

[7]. Doraivelu S M, Gegel H L，Gunasekera J, "A New Yield Function for Compressible P/M Materials Journal", International Journal of Mech. Set., 1984, Volume 26, No.9, pp 527-535.

[8]. Kim H S, Won C W, Chun B S "Plastic Deformation of Porous Metal with an Initial Inhomogeneous Density Distribution", Journal of Materials Processing Technology, 1998, Volume 74 pp 213-237.

[9]. Lippmann H, Iankov R. "Mathematical Modeling of Sintering During Powder Forming Processes", International Journal of Mechanical Sciences ,1997 Volume 39 No.5 pp585-596.

[10]. HUA Lin, ZHAO Zhongzhi, "Experimental Study on Filling Cavity Process of Powder Sintering Material" Journal of Die and Mould Technology, 1999, Volume 1pp 22-24.

[11]. HUA Lin, Qin Shunpeng, MAO Huajie, ZHAO Yumin, "The Plastic Deformation and Yield Criterion for Compressible Sintered Powder Material," Journal of Plasticity Engineering, 2003，Volume 10 No.6 pp 62-65.

[12]. HUA Lin, ZHAO Zhongzhi, "Plastic Theory and Application of Sintering Material", Journal of Mechanism Engineering, 1992 Volume 28, No. 4 pp 94-101.

[13]. M. Asif, K. Chandra, P.S. Misra, "Mechanical Properties of Powder Based Steel used as Backing Plate in Heavy Duty Brake Pad Manufacturing", Journal of Minerals & Materials Characterization & Engineering, Volume 11, No.5, 2012.pp.509-518,

[14]. Gaungchun Wang and Guogun ZHAO , "Powder Forging of a Motorcycle Connecting rod", Journal of Material Science Technology, Volume 18, N0.6 2002 –, pp 544-548 .

[15]. Bruce Lindsley, Hoeganaes Corporation, Cinnaminson, NJ 08077 USA, "Alloy Development of Sinter-Hardenable Compositions", Presented at Euro PM2007, Toulouse, France 15-18 October. http://www.gkn.com/hoeganaes/media/Tech Library/199.

[16]. efunda – Online Resource " Application of AISI 8620 Steels" Sunnyvale.

[17]. Narayanasamy R, Pandey K.S., "Some Aspects of Work Hardening in Sintered Aluminium - Iron Composite Preform during Cold Axial forming" , Journal of Material Process Technology 1998, Volume 84 pp136 -142.

[18]. K.S.Pandey, R.Narayanasamy and V. Senthilkumar, "Some Aspects on Hot Forging Features of P/M Sintered Iron Preforms under Various Stress State Conditions", Elsevier, Mechanics of Materials, Volume 38, 2006 pp 376-386.

[19]. K.Manisekar and R.Narayanasamy "Effect of Friction on Barrelling in Square and Rectangular Billets of Aluminium during Cold Upset Forging," Elsevier, Materials and Design, Volume 28, 2007, pp 592-598.